Journal of Plastic, Reconstructive & Aesthetic Surgery (2019) 72, 1484–1493

JPRAS
An International Journal of Surgical Reconstruction
www.JPRASurg.com

Cancer stem cells within moderately differentiated head and neck cutaneous squamous cell carcinoma express components of the renin-angiotensin system☆

Shanella Nallaiah[a], Valerie Ming Yi Lee[a], Helen D Brasch[a], Jennifer de Jongh[a], Bede van Schaijik[a], Reginald Marsh[a,b], Swee T Tan[a,c,1,*], Tinte Itinteang[a,1]

[a] *Gillies McIndoe Research Institute, PO Box 7184, Newtown, Wellington 6242, New Zealand*
[b] *Auckland University, Private Bag 92019, Victoria St, West Auckland 1142, New Zealand*
[c] *Wellington Regional Plastic, Maxillofacial & Burns Unit, Hutt Hospital, Private Bag 31709, Lower Hutt, New Zealand*

Received 5 September 2018; accepted 18 November 2018

KEYWORDS
Head and neck;
Cutaneous;
Squamous cell carcinoma;
Cancer;
Stem cell;
Renin-angiotensin system

Summary *Purpose:* To investigate the expression of components of the renin-angiotensin system (RAS): pro-renin receptor (PRR), angiotensin converting enzyme (ACE), angiotensin II receptor 1 (ATIIR1) and angiotensin II receptor 2 (ATIIR2) by the cancer stem cell (CSC) sub-populations in moderately differentiated head and neck cutaneous squamous cell carcinoma (MDHNCSCC).
Methodology: 3,3-Diaminobenzidine (DAB) immunohistochemical (IHC) staining for PRR, ACE, ATIIR1 and ATIIR2 was performed on formalin-fixed paraffin-embedded sections of ten MDHNC-SCC tissue samples. Immunofluorescence (IF) IHC staining was used to localise components of the RAS. Western blotting (WB) and RT-qPCR were performed on snap-frozen MDHNCSCC tissue samples and MDHNCSCC-derived primary cell lines to investigate protein transcription expression of these proteins, respectively.

☆ Part of this article have been presented at the following conferences: 1. The 87th Royal Australasian College of Surgeons' Annual Scientific Congress with the American College of Surgeons and the Australian and New Zealand College of Anaesthetists Annual Scientific Meeting, Sydney, Australia, May 7–11, 2018. 2. The Australian and New Zealand Head and Neck Cancer Society and the 15th Meeting of the International Society for Maxillofacial Rehabilitation, July 26–28, 2018, Melbourne, Australia.

[1] Both are equal senior authors.

* Corresponding author at: Gillies McIndoe Research Institute, PO Box 7184, Newtown, Wellington 6242, New Zealand.
E-mail address: swee.tan@gmri.org.nz (S.T. Tan).

https://doi.org/10.1016/j.bjps.2018.11.013
1748-6815/© 2018 British Association of Plastic, Reconstructive and Aesthetic Surgeons. Published by Elsevier Ltd. All rights reserved.

Results: DAB IHC staining demonstrated the presence of PRR, ACE, ATIIR1 and ATIIR2 in all ten MDHNCSCC tissue samples. IF IHC staining showed expression of PRR and ATIIR2 by the $OCT4^+$ cells, and ACE and ATIIR1 by the $SOX2^+$ cells, within the tumour nests (TNs) and the peritumoural stroma (PTS). PRR, ACE, ATIIR1 and ATIIR2 were expressed by the endothelium of the microvessels within the PTS. WB confirmed protein expression for PRR, ACE and ATIIR1 in MDHNCSCC tissue samples and MDHNCSCC-derived primary cell lines. RT-qPCR showed transcriptional activation of PRR, ACE, ATIIR1 and ATIIR2 in MDHNCSCC tissue samples; and PRR, ACE, ATIIR1 but not ATIIR2, in MDHNCSCC-derived primary cell lines.
Conclusion: PRR, ACE, ATIIR1 and ATIIR2 are expressed by the CSC subpopulations within the TNs, the PTS, and the endothelium of the microvessels within the PTS, in MDHNCSCC.
© 2018 British Association of Plastic, Reconstructive and Aesthetic Surgeons. Published by Elsevier Ltd. All rights reserved.

Introduction

The incidence of non-melanoma skin cancer has been increasing worldwide[1] with cutaneous squamous cell carcinoma (CSCC) being the second most common and 60% affecting the head and neck.[2] In New Zealand, the incidence of CSCC has been rising at a 1.1% annual rate over eight years, particularly amongst the aging population.[1]

Ultraviolet (*UV*) radiation exposure is the major cause for CSCC through several mechanisms,[1] with most CSCCs located on sun-exposed skin, mainly the head and neck, especially in fair-skinned individuals.[3] Other risk factors include human papillomavirus infection, chronic immunosuppression and chronic conditions.[4]

The cancer stem cell (CSC) concept of carcinogenesis proposes CSCs as the origin of cancer[5] which have a unique capability to maintain cancer.[5] Current research focuses on the hierarchical organisation of CSCs, with the most primitive subpopulation possessing pluripotency atop the hierarchy, differentiating to mature cancer cells.[6] Both CSCs and non-CSCs show plasticity, capable of transforming their phenotype in response to certain stimuli.[7]

Resistance of CSCs to radiotherapy and chemotherapy could explain cancer relapse following clinical remission.[8] CSCs can be distinguished from the bulk of the cancer cells by their expression of specific embryonic stem cell (ESC) markers.[9] More invasive tumours overexpress these ESC markers.[9, 10] Although several markers are associated with CSCs, OCT4, SOX2, KLF4, NANOG and c-MYC, are more crucial to the induction and maintenance of their ESC-like phenotype.

We have recently demonstrated the presence of an $OCT4^+/NANOG^+/SOX2^+/KLF4^+/c\text{-}MYC^+$ CSC subpopulation localised to the tumour nests (TNs), the peritumoural stroma (PTS), and the endothelium of the microvessels within the PTS of MDHNCSCC, and also a $OCT4^+/NANOG^-/SOX2^+/KLF4^+/c\text{-}MYC^+$ subpopulation within the PTS.[11]

The renin-angiotensin system (RAS) physiologically maintains blood pressure and blood volume.[12] Angiotensinogen (AGN) is activated to form angiotensin I (ATI) by renin, which is converted from pro-renin by binding to pro-renin receptor (PRR).[12] Angiotensin converting enzyme (ACE) converts ATI to angiotensin II (ATII). ATII acts on ATII receptor 1 (ATIIR1) or ATII receptor 2 (ATIIR2) to produce a number of physiological effects in target tissues.[13]

Dysregulation of the RAS leads to a broad range of pathological effects. Components of the RAS are overexpressed in several cancer types, and have been localised to CSCs.[14] Furthermore, components of the RAS are known to be expressed in many different cell types within the tumour microenvironment, including endothelial cells, fibroblasts and an array of immune cells.[15] The ACE/ATII/ATIIR1 axis promotes tumour growth by modulating angiogenesis, inflammation and desmoplasia.[16] Conversely, the ATII/ATIIR2 axis confers a protective effect against carcinogenesis.[16] RAS modulators mitigate tumour growth and spread and improve outcome of cancer patients.[17]

This study investigated the expression of the components of the RAS: PRR, ACE, ATIIR1 and ATIIR2 in MDHNCSCC tissue samples and cell lines derived directly from these tissue samples, using 3,3′-diaminobenzidine (DAB) and immunofluorescence (IF) immunohistochemical (IHC) staining, Western blotting (WB) and real-time polymerase chain reaction (RT-qPCR).

Materials and methods

MDHNCSCC tissue samples

MDHNCSCC tissue samples (MDHNCSCCTS) from 9 male and 1 female patients, aged 60–93 (mean, 77.3) years, included in our recent study,[11] were sourced from the Gillies McIndoe Research Institute Tissue Bank for this study, which was approved by the Central Health and Disability Ethics Committee (Ref. no. 12/CEN/74). Written informed consent was obtained from patients included in this study.

MDHNCSCC-derived primary cell lines

Primary cell lines were derived directly from six fresh MDHNCSCCTS from the ten patients used for DAB IHC staining, as described.[18] Cells were cultured in DMEM media with high glucose and containing pyruvate (cat#10569010, Thermo Fisher Scientific, Waltham, MA, USA), supplemented with 10% FCS (cat#10091148, Thermo Fisher Scientific), 5% mTeSR™1 (cat#85850, Stemcell Technologies, Vancouver, Canada), 1% penicillin-streptomycin (cat#15140122, Thermo Fisher Scientific) and 0.2% gentamicin/amphotericin B (Cat# R01510, Thermo Fisher Scientific). Cultures were maintained in a humidified incubator with 5% CO_2 at 37 °C.

Histochemical and immunohistochemical staining

Haematoxylin and eosin (H&E) staining was performed on 4 μm-thick formalin-fixed paraffin-embedded sections of MDHNCSCCTS from ten patients. Each HNMDCSCC was identified and the histological grade confirmed by an anatomical pathologist (HDB). DAB IHC staining was performed on sections of the HNMDCSCCTS using primary antibodies for PRR (1:2000; cat#ab40790, Abcam, Cambridge, MA, USA), ACE (1:100; cat#MCA2054, AbD Serotec, Raleigh, NC, USA), ATIIR1 (1:30; cat#ab9391, Abcam), ATIIR2 (1:2000; cat#NBP1-77368, Novus Biologicals, Littleton, CO, USA), SOX2 (1:200; cat#PA1-094, Thermo Fisher Scientific, Rockford, IL, USA) and OCT4 (1:30; cat#MRQ-10, Cell Marque). All antibodies were diluted with Bond™ primary antibody diluent (cat#AR9352, Leica). Surgipath Micromount mounting medium (cat#38017322, Leica) was used to mount all slides.

To determine co-expression of the proteins, IF IHC staining was performed on three MDHNCSCCTS from the original cohort of ten patients used for DAB IHC staining. Dual staining was performed using identical primary antibodies and concentrations as used for DAB IHC staining, with primary antibodies for ERG (1:200; cat#EP111, Cell Marque), an endothelial marker. For detection of the primary antibody, an appropriate fluorescent secondary antibody of Vectafluor Excel anti-mouse (ready-to-use; cat#VEDK2488, Vector Laboratories, Burlingame, CA, USA) or Alexa Fluor anti-rabbit 594 (1:500; cat#A21207, Life Technologies, Carlsbad, CA, USA) was used. IF IHC-stained slides were mounted in Vectashield HardSet anti-fade mounting medium and counterstained with 4′6-diamino-2-phenylinodole (cat#H-1500, Vector Laboratories). All IF IHC-stained slides were mounted in Vecta Shield Hardset mounting medium with 4′,6′-diamidino-2-phenylindole (Vector Laboratories). Human tissues used for positive controls were placenta for PRR, liver for ATIIR1 and kidney for ATIIR2 and ACE. To determine the specificity of the amplification cascade used in DAB IHC staining, negative controls were performed on sections of MDHNCSCC using a matched isotype control for both mouse (ready-to-use; cat#IR750, Dako, Copenhagen, Denmark) and rabbit (ready-to-use; cat#IR600, Dako) primary antibodies. Negative controls for IF IHC staining were performed using a combination of primary isotype mouse (ready-to-use; cat#IR750, Dako) and rabbit (ready-to-use; cat#IR600, Dako) antibodies.

Image analysis

DAB IHC-stained slides were visualised and imaged using the Olympus BX53 light microscope, fitted with an Olympus SC100 digital camera, and processed with the CellSens 2.0 Software (Olympus, Tokyo, Japan). IF IHC-stained slides were viewed and imaged with the Olympus FV1200 biological confocal laser-scanning microscope, and processed with CellSens Dimension 1.11 software using 2D deconvolution algorithm (Olympus).

RT-qPCR

RNA was extracted from 20 mg each of the five snap-frozen MDHNCSCCTS from the original cohort of ten patients used for DAB IHC staining. Tissue sections were each suspended in 350 μL lysis buffer RLT (cat#79216, Qiagen, Hilden, Germany). Samples were homogenised using the Omni Tissue Homogenizer (Omni International, Kennesaw, GA, USA). The RNeasy Mini Kit (Qiagen) and the QIAcube (Qiagen) were used for RNA extraction, and quantified using the NanoDrop 2000 Spectrophotometer (Thermo Fisher Scientific). Four MDHNCSCC-derived primary cell lines (MDHNCSCCPCL) were subject to the same RNA extraction process.

Extracted samples underwent RT-qPCR using the Rotor-Gene Q (Qiagen) and the Rotor-Gene Multiplex RT-PCR Kit (Qiagen). The primer probes used were PRR (Hs00997145_m1), ACE (Hs00174179_m1), ATIIR1 (Hs00258938_m1) and ATIIR2 (Hs02621316_s1). All probes were obtained from Thermo Fisher Scientific (cat#4331182). Threshold cycle values were compared against the housekeeper GAPDH (Hs99999905_m1) (cat#4351370, Thermo Fisher Scientific).

Western blotting

Total protein was extracted and precipitated from five snap-frozen MDHNCSCCTS and six MDHNCSCCPCL, from the original cohort of ten patients used for DAB IHC staining, and separated by SDS-PAGE and transferred to a PVDF membrane using methods previously described.[19] Protein detection was performed on the iBind Flex (cat#SLF2000, Thermo Fisher Scientific) using the primary antibodies for PRR (ATP6IP2, 1:500, cat#ab40790, Abcam, Cambridge, UK), ATIIR1 (AT2R1, 1:500; cat#sc-1173, Santa Cruz, CA, USA), ATIIR2 (1:500; cat#ab92445, Abcam), ACE (1:200; cat#sc-12184, Santa Cruz), and α-tubulin (1:1000; cat#62204, Thermo Fisher Scientific). Appropriate secondary antibodies were goat anti-rabbit HRP (1:1000, cat#A16110, Thermo Fisher) and donkey anti-rabbit HRP (1:1000, cat#SA1-200, Thermo Fisher) for PRR, ATIIR1 and ATIIR2, and goat anti-mouse Alexa Fluor 488 (1:2000; cat#A21202, Life Technologies) for α-tubulin. ACE tertiary cascade used a rabbit anti-goat Superclonal™ biotin conjugated secondary antibody (1:4000; cat#A27013, Thermo Fisher) followed by a Pierce™ Streptavidin Poly HRP (1:5000, cat#21140, Thermo Fisher) at 4 °C for 10 min. Clarity Western ECL (cat#1705061, Bio-Rad) was used as the substrate for visualising HRP detected protein bands and the ChemiDoc MP Imaging System (Bio-Rad) and Image Lab 6.0 software (Bio-Rad) were used for band detection and analysis. Positive controls were human placenta for PRR and ATIIR1, mouse lung for ACE, and a recombinant ATIIR2 protein (cat#H00000186-P01, Novus Biologicals, Littleton, CO, USA) for ATIIR2. Matched mouse (1:500; cat#ab18443, Abcam) and rabbit (1:500; cat#ab171870, Abcam) isotype controls were used as appropriate negative controls.

Statistical analyses

The data obtained from the MDHNCSCCTS and MDHNCSCCPCL were first transformed by Log_{10} and then the Wilcoxon Matched Pairs Signed Ranks test was applied. The analysis package was SPSS v24. The analysis performed on data obtained from the cell lines was performed using student's *t*-test for paired samples.

Results

Histochemical and 3,3′-diaminobenzidine immunohistochemical staining

H&E staining confirmed the presence and appropriate histological grade for all ten MDHNCSCCTS, displaying tumour nests (TNs) and with intervening peritumoural stroma (PTS) (Suppl. Figure 1A). DAB IHC staining showed membranous and cytoplasmic expression of PRR (Figure 1A, brown) by the cells within the TNs and cytoplasmic expression on the cells within the PTS. ACE (Figure 1B, brown) was predominantly localised to the endothelium of the microvessels within the PTS. ATIIR1 (Figure 1C, brown) demonstrated cytoplasmic and nuclear expression throughout the PTS and the endothelium of the microvessels within the PTS, and moderate cytoplasmic and nuclear staining throughout the TNs. ATIIR2 (Figure 1D, brown) displayed weak granular cytoplasmic expression on the cells within the TNs and the PTS.

Human tissues used for positive controls demonstrated the expected staining patterns for PRR (Suppl. Figure 1B, brown) in placenta, ACE (Suppl. Figure 1C, brown) in kidney, ATIIR1 (Suppl. Figure 1D, brown) in liver, and ATIIR2 (Suppl. Figure 1E, brown) in kidney. The omission of the primary antibodies in HNMDCSCCTS provided the negative controls for all DAB IHC-stained slides (Suppl. Figure 1F).

Immunofluorescence immunohistochemical staining

We have recently demonstrated, within HNMDCSCC, the presence of an $OCT4^+/NANOG^+/SOX2^+/KLF4^+/c\text{-}MYC^+$ CSC subpopulation within the TNs, the PTS, and the endothelium of the microvessels within the PTS; and an $OCT4^+/NANOG^-/SOX2^+/KLF4^+/c\text{-}MYC^+$ CSC subpopulation within the PTS.[11] ACE (Figure 2A, green) was expressed by the $SOX2^+$ (Figure 2A, red) CSC subpopulation within the PTS, as well as the ERG^+ (Figure 2B, red) endothelium of the microvessels. ATIIR1 (Figure 2C, green) was detected on the $SOX2^+$ (Figure 2C, red) CSC subpopulation within the TNs and the PTS, and the ERG^+ (Figure 2D,

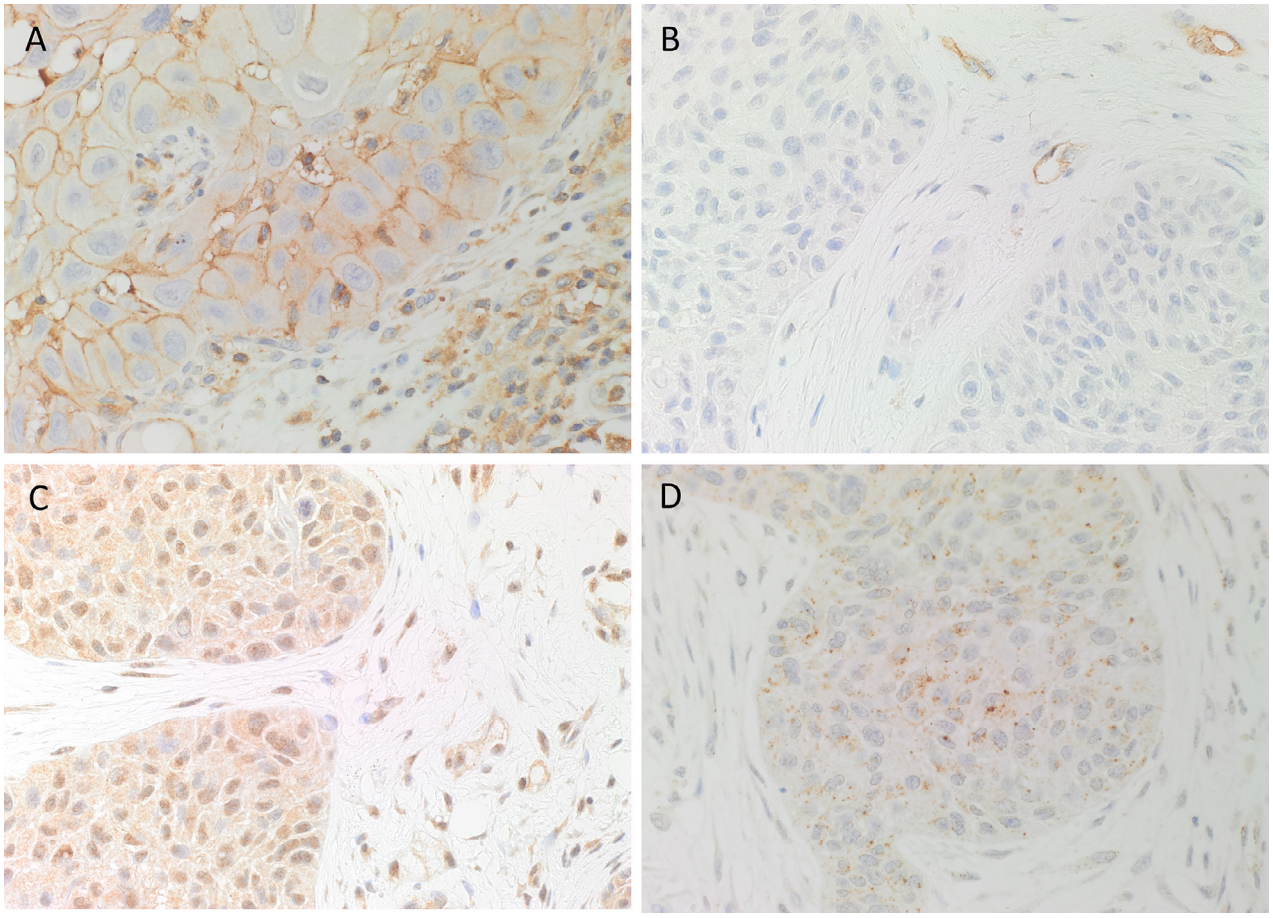

Figure 1 Representative 3,3-diaminobezidine immunohistochemical-stained sections of moderately differentiated head and neck cutaneous squamous cell carcinoma tissue samples demonstrating expression of PRR (A, brown) by cells within the tumour nests (TNs) and the peritumoural stroma (PTS), and the endothelium of the microvessels within the PTS. ACE was exclusively expressed by the endothelium of the microvessels (B, brown). ATIIR1 (C, brown) and ATIIR2 (D, brown) were expressed by cells within the TNs and the endothelium of the microvessels within the PTS, but ATIIR2 had comparatively lighter staining throughout. Nuclei were counter-stained with haematoxylin (A–D, blue]. Original magnification: 400×.

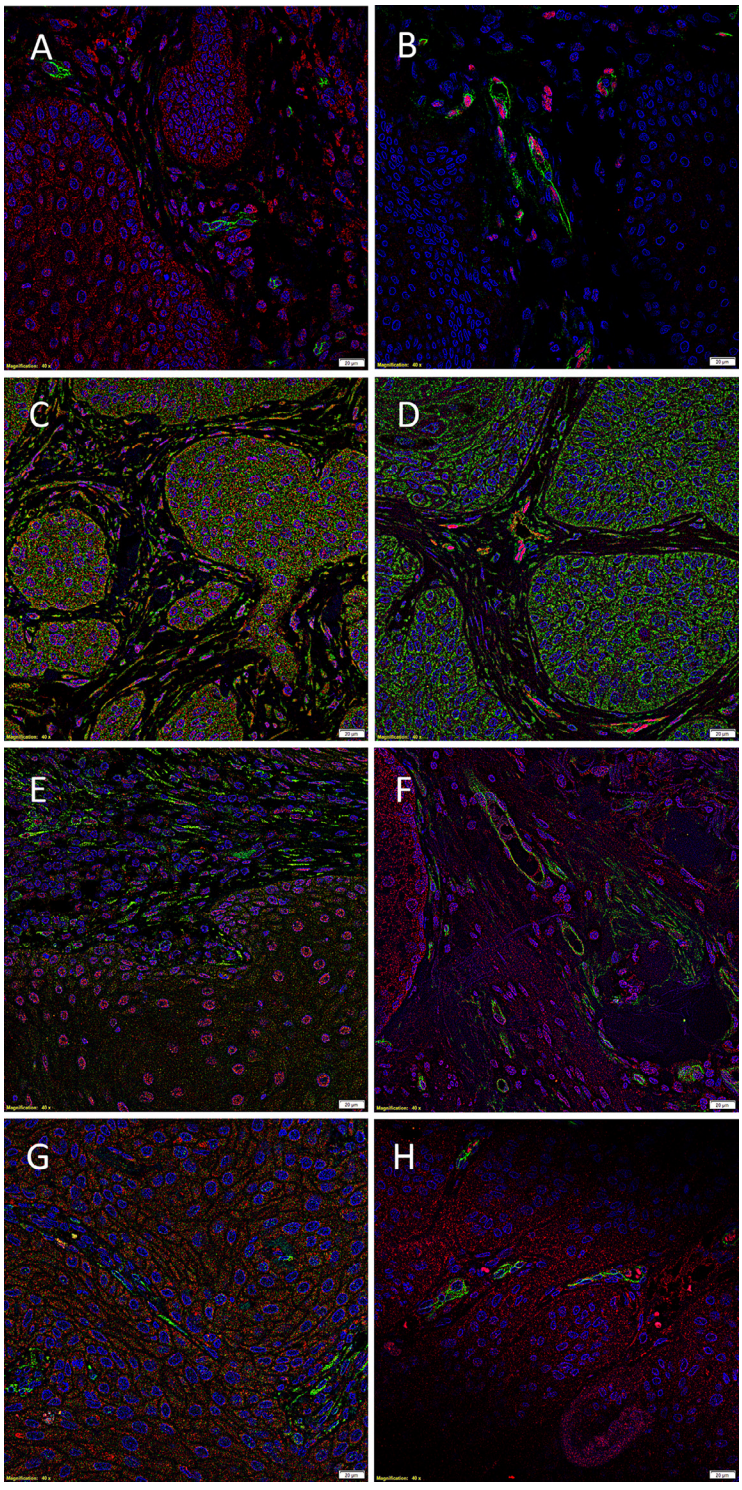

Figure 2 Representative immunofluorescence immunohistochemical-stained sections of moderately differentiated head and neck cutaneous squamous cell carcinoma tissue samples demonstrating expression of ACE (A,B, green) by the $SOX2^+$ (A, red) cells within the peritumoural stroma (PTS), and the ERG^+ (B, red) endothelium of the microvessels within the PTS. ATIIR1 (C,D, green) was detected in the $SOX2^+$ (C, red) CSC subpopulation within the tumour nests (TNs) and the PTS and the ERG^+ (D, red) endothelium of the microvessels within the PTS. Faint staining of ATIIR2 (E,F, red) was present in the $OCT4^+$ (E, green) CSC subpopulation throughout the TNs and the PTS, and the $CD34^+$ (F, green) endothelium of the microvessels within the PTS. Abundant expression of PRR (G, red) was demonstrated on the $OCT4^+$ (G, green) CSC subpopulation within the TNs and the PTS. PRR (H, red) was also expressed by the $CD34^+$ (H, green) endothelium of the microvessels within the PTS. Cell nuclei were counterstained with 4′,6′-diamidino-2-phenylindole (A–H, blue). Original magnification 400×.

red) endothelium of the microvessels within the PTS. Faint staining of ATIIR2 (Figure 2E, red) was present on the OCT4$^+$ (Figure 2E, green) CSC subpopulation throughout the TNs and the PTS, and the CD34$^+$ (Figure 2F, green) endothelium of the microvessels within the PTS. Abundant expression of PRR (Figure 2G,H, red) was demonstrated on the OCT4$^+$ (Figure 2G, green) CSC subpopulation within the TNs and the PTS, and the CD34$^+$ (Figure 2H, green) endothelium of the microvessels within the PTS.

Images demonstrating individual stains of the merged images in Figure 2 are provided in Supplementary Figure 2. Specificity of primary antibodies was confirmed on the negative controls (Suppl. Figure 2Q), which demonstrated minimal staining.

RT-qPCR

RT-qPCR, normalised against the housekeeper GAPDH, confirmed transcription activation of PRR, ACE, ATIIR1 and ATIIR2 across all six snap-frozen MDHNCSCCTS (Figure 3). ΔCt values were transformed using Log_{10} and then the Wilcoxon Matched Pairs Signed Ranks test was applied. This showed that PRR significantly higher expression of ACE: ACE ($p < 0.028$); ATIIR1 ($p < 0.028$) and ATIIR2 ($p < 0.046$). ACE was significantly less expressed than ATIIR1 ($p < 0.028$) but not significantly different from ATIIR2 ($p < 0.600$). The expression of ATIIR1 was not significantly different from that of ATIIR2 ($p < 0.075$).

RT-qPCR performed on five MDHNCSCCPCL, for PRR, ACE, ATIIR1 and ATIIR2, normalised against the housekeeper GAPDH, confirmed the presence of PRR, ACE and ATIIR1 across all five samples, with ATIIR2 being below detectable levels (Figure 4). ΔCt values were transformed using Log_{10} and then the student's *t*-test was applied to compare paired samples. This showed that the relative abundance of PRR and the following markers is significant: ACE ($p < 0.000$); ATIIR1 ($p < 0.002$) and ATIIR2 ($p < 0.000$). ACE was significantly more abundantly expressed than ATIIR2 ($p < 0.000$) but only marginally significantly different from ATIIR1 ($p < 0.056$). There was no significant difference between the expression of ATIIR1 and ATIIR2 ($p < 0.075$).

Western blotting

WB on five snap-frozen MDHNCSCCTS demonstrated the presence of bands at the expected molecular weights for PRR, ACE and ATIIR1 (Figure 5). PRR was detected in four out of five tissue samples (Figure 5A, red), as two bands

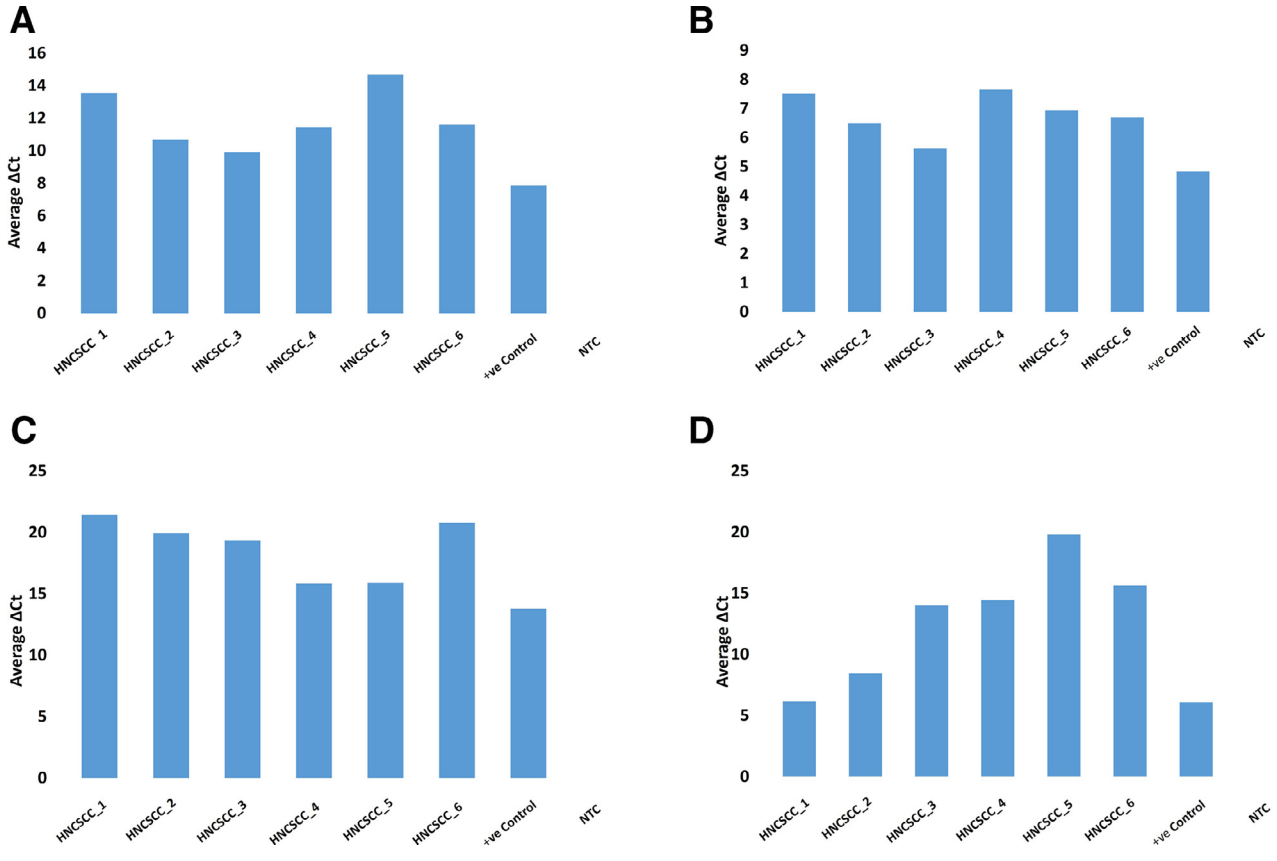

Figure 3 Graphs showing average ΔCT values of triplicate RT-qPCR runs performed on snap-frozen moderately differentiated head and neck cutaneous squamous cell carcinoma tissue samples, amplifying transcripts for ACE (A), PRR (B), ATIIR1 (C) and ATIIR2 (D). ΔCT was calculated by comparing CT values of components of the renin-angiotensin system to that of housekeeping gene GADPH. Positive controls are confirmed on human fibroid tissue, and specificity of the probe is demonstrated using a no template control (NTC).

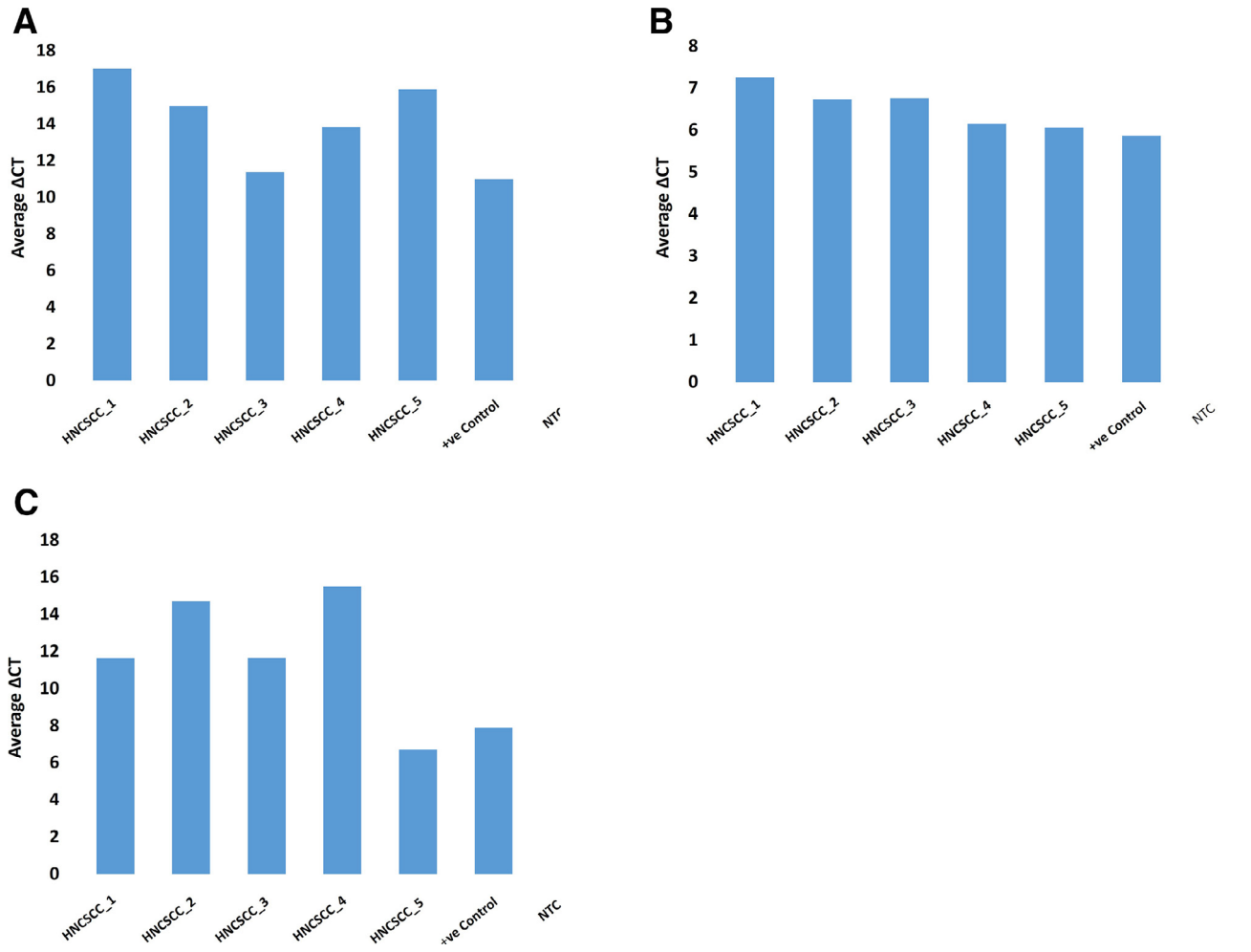

Figure 4 Primary cell lines derived from five moderately differentiated head and neck cutaneous squamous cell carcinoma tissue samples subjected to RT-qPCR, demonstrating transcript expression of ACE (A), PRR (B), ATIIR1 (C) and ATIIR2 (D). ΔCT values calculated by comparing CT values of the components of the RAS to that of housekeeping gene GAPDH, with graphs displaying average ΔCT values of triplicate trials run on each sample. Positive controls were demonstrated on uterine fibroid tissue, and specificity of probe confirmed using a no template control (NTC).

at the appropriate weights of 21 kDa and 35 kDa, representing the soluble form and the transmembrane form respectively.[20] ATIIR1 was detected at the appropriate molecular weight of 41 kDa[14] in four out of the five tissue samples with specificity confirmed on placenta tissue (Figure 5B, red). ATIIR2 was below detectable levels in all five tissue samples (Figure 5C, red). ACE was detected at the molecular weight of 194 kDa[14] in two out of the five MDHNCSCCTS with the specificity of the antibody confirmed by mouse lung as the control tissue (Figure 5D, red). Bands for α-tubulin (Figure 5E, green) confirmed approximate equivalent protein loading for all MDHNCSCCTS examined. The rabbit and mouse IgG isotype controls (Suppl. Figure 3A) were used to detect any non-specific staining.[14, 20, 21]

WB on the six MDHNCSCCPCL demonstrated the presence of bands at the expected molecular weights for PRR and ATIIR1 but not ATIIR2 or ACE (Figure 6). PRR was detected in five out of six cell lines (Figure 6A, red) at 21 kDa and at approximately 70 kDa representing dimerisation of PRR, possibly induced by renin binding.[19] ATIIR1 was detected at the appropriate molecular weight of 41 kDa (Figure 6B, red) with specificity confirmed in placenta tissue. ATIIR2 was not detected (Figure 6C) at the expected molecular weight of 40 kDa, with specificity of the antibody confirmed by recombinant ATIIR2 protein which demonstrated detection of a band at the expected molecular weight of 55 kDa. ACE was not detected in any of the MDHNCSCCPCL (Figure 6D). Bands for α-tubulin confirmed approximate equivalent protein loading for all MDHNCSCCTS examined (Figure 6E). The rabbit and mouse IgG isotype controls (Suppl. Figure 3B) were used to detect any non-specific staining.

Discussion

The RAS has been implicated in many pathological states, with recent studies highlighting the association between RAS dysregulation and carcinogenesis, most significantly the ACE/ATII/ATIIR1 axis.[17] Its paracrine actions entail a complex interaction within several key cell-signalling pathways,

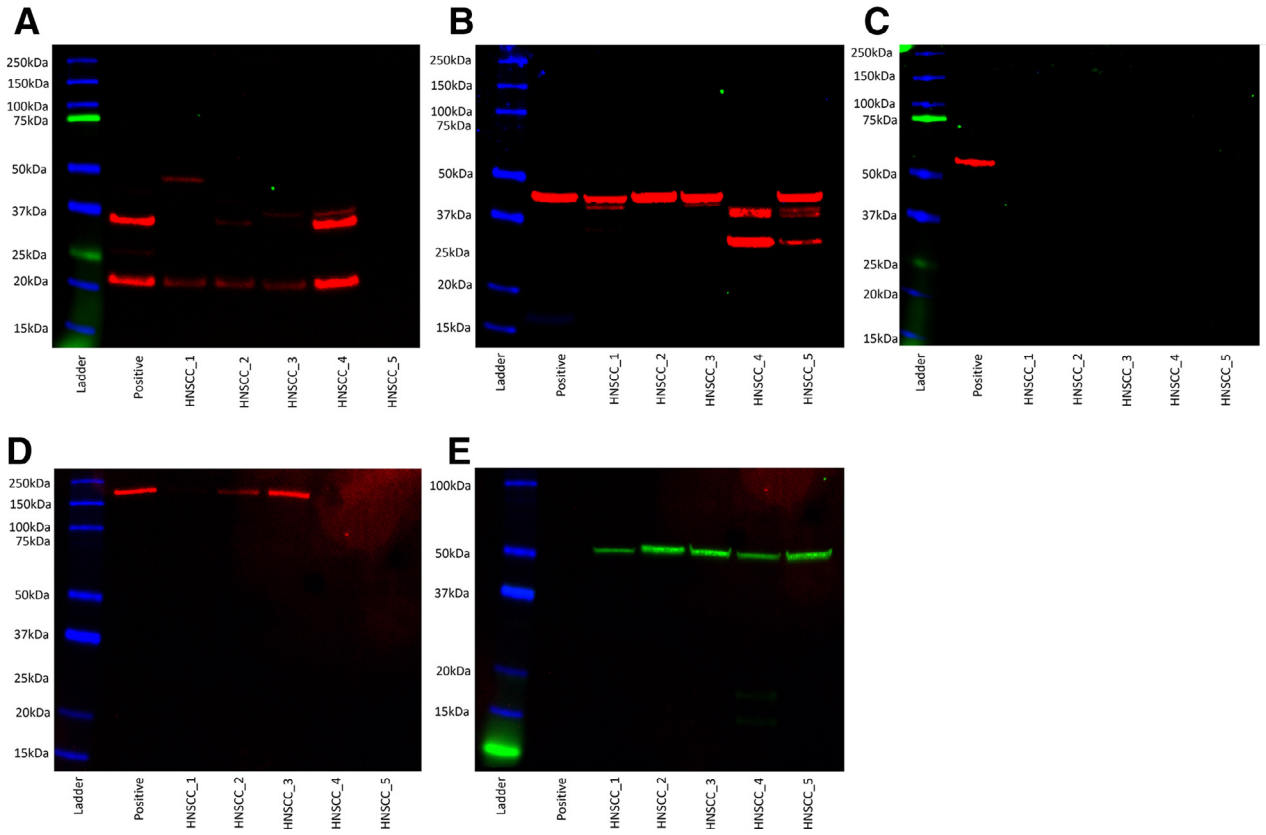

Figure 5 Western Blot (WB) images of total protein extracted from five moderately differentiated head and neck cutaneous squamous cell carcinoma tissue samples probed for PRR (A), ATIIR1 (B), ATIIR2 (C) and ACE (D). WB for α-tubulin (E) which was used as a housekeeping protein. The molecular weight ladder (kDa) is labelled for each blot.

thus attenuating carcinogenesis by modulating the tumour microenvironment, particularly sustaining angiogenesis, cell migration and pro-survival signalling.[22, 23]

We have recently demonstrated the presence of an $OCT4^+/NANOG^+/SOX2^+/KLF4^+/$ $c\text{-}MYC^+$ CSC subpopulations localised to the TNs, the PTS, and the endothelium of the microvessels within the PTS in MDHNCSCC; and an $OCT4^+/NANOG^-/SOX2^+/KLF4^+/c\text{-}MYC^+$ CSC subpopulation within the PTS.[11] In this study we have demonstrated expression of PRR, ACE, ATIIR1 and ATIIR2 by the $OCT4^+/SOX2^+$ CSC subpopulations.

PRR, ATIIR1 and ATIIR2 were demonstrated throughout the tumour microenvironment – within the TNs, the PTS and the endothelium of the microvessels within the PTS in all ten MDHNCSCCTS by DAB IHC staining. This was confirmed by the presence of transcription activation of these proteins within the tissue samples. However, mRNA and protein expression of ATIIR2 was below detectable levels within the MDHNCSCCPCL by RT-qPCR and WB analyses, respectively. This may be due to MDHNCSCCPCL not expressing ATIIR2 having differentiated down a cellular pathway that does not express the aforementioned proteins. This finding is consistent with several studies showing ATIIR2 playing a cancer-protective role counteracting the downstream carcinogenic effects of ATIIR1 activation.[16] ATIIR2 opposes tumour angiogenesis through inhibition of the vascular endothelial growth factor (VEGF) pathway, and hence low expression in a carcinogenic tumour *niche*.[6] However, our finding of ATIIR2 within the tissue samples supports other studies suggesting that ATIIR2 may possess a pro-carcinogenic effect, parallel to the ATII/ATIIR1 axis.[24]

Similarly, ACE was below detectable levels in the MDHNCSCCPCL. This may be attributed to the cell line constituents not directly reflecting the composition of the tissues. Interestingly, IF IHC staining demonstrated localisation of ACE only to the endothelium of the microvessels within the PTS. This could reflect 'vascular mimicry' and the involvement of ACE in promoting tumour angiogenesis.[25] Interestingly, comparable expression patterns of ACE are found in a primitive phenotypic endothelium found in close proximity to colorectal cancer.[26] This may imply that ACE plays a role in regulating epithelial-to-mesenchymal transition (EMT), a process central to cancer metastasis, by promoting tumour angiogenesis.[16, 26, 27] Different alleles of ACE affects cancer prognosis, with homozygotes for II and AA alleles yielding low-activity isotypes of ACE which interestingly lead to a phenotype with low incidences of cancer.[28] Whereas DD and TT homozygotes have been shown to have a high-activity form of ACE which correlated with higher incidence of cancer.[28]

ATIIR1 was the most ubiquitously expressed component of the RAS within all three areas of the tumour microenvironment. The association of ATIIR1 with cancer progression has been widely observed. Overexpression of ATIIR1 in cutaneous and lip SCC and a correlation between increased expression and worsening tumour differentiation

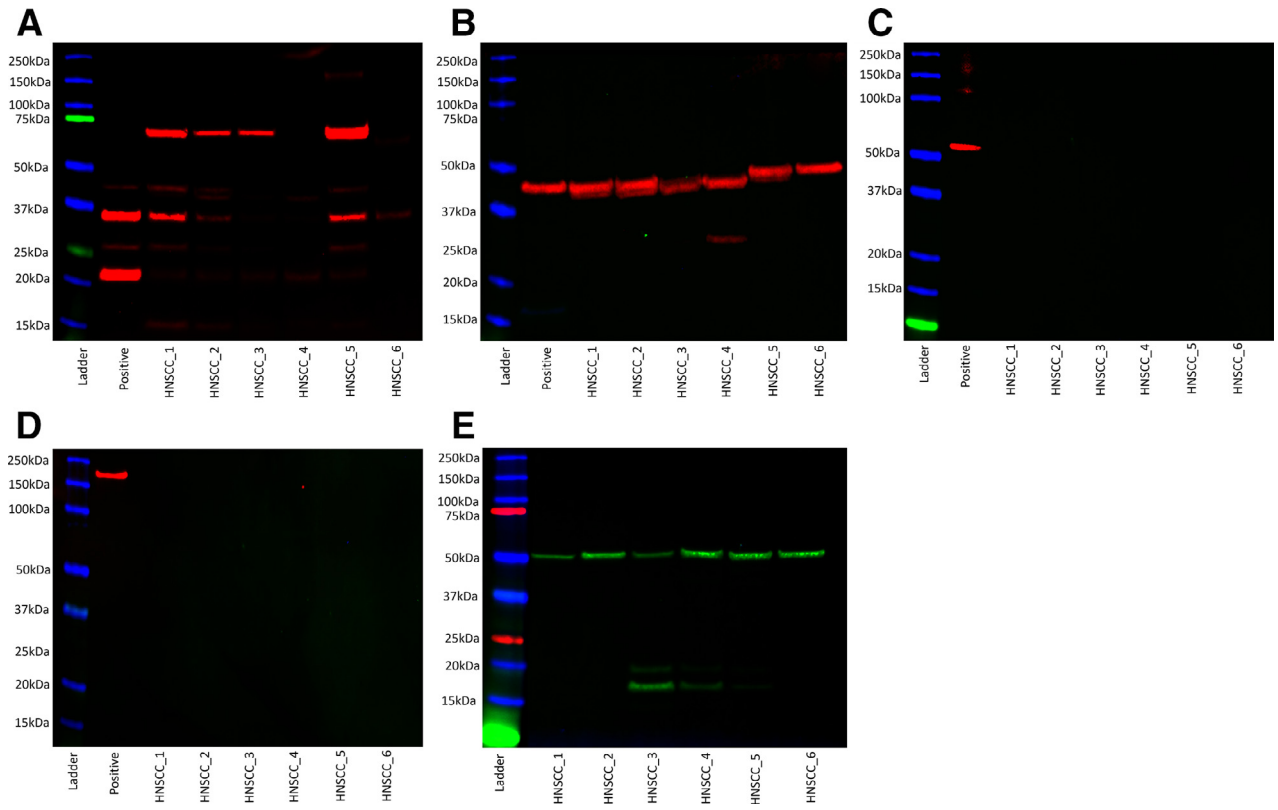

Figure 6 Western Blot (WB) images of total protein extracted from primary cell lines derived from six moderately differentiated head and neck cutaneous squamous cell carcinoma samples probed for PRR (A), ATIIR1 (B), ATIIR2 (C) and ACE (D). WB for α-tubulin (E) which was used as a housekeeping protein. The molecular weight ladder (kDa) is labelled for each blot.

have demonstrated.[29] VEGF signalling is increased by ATIIR1, thus contributing to the increased aptitude for angiogenesis displayed by tumours. Furthermore, the interaction of ATII with ATIIR1 also promotes EMT alongside the effects of ACE.[30]

PRR has been suggested to play a vital role in the proliferation of CSCs, mainly through its role in the Wnt/β-catenin signalling pathway resulting in accelerated carcinogenesis.[20] We have observed the presence of PRR within all aspects of the tumour microenvironment, with particular abundance within the TNs. The presence of PRR on the endothelium of the microvessels also implicates PRR in EMT and cancer progression.[31]

These novel findings are consistent with our previous studies in buccal mucosal,[32] oral tongue,[33] lip[14] SCC, and glioblastoma.[34] We speculate that CSCs may be a novel therapeutic target by modulation of the RAS using existing medications such as aliskerin, a renin inhibitor; β-blockers, which block the production of pro-renin and thus reduce renin levels; ACE inhibitors and ATII receptor 1 blockers (ARBs), show promise as an alternative approach to MDHNCSCC therapy.[35–37] Users of ACE inhibitors or ATIIR1 blockers have a lower incidence of SCC than non-users, and thus it is exciting to infer similar results for MDHNCSCC.[38]

Acknowledgements

We thank Ms Liz Jones and Ms Erin Paterson of the Gillies McIndoe Research Institute for their assistance in IHC staining and cell culture, respectively. SN and VL were supported by summer scholarships from the Deane Endowment Trust.

Conflicting interests

The authors declare that the research was conducted in the absence of any commercial or financial relationships that could be construed as a potential conflict of interest. TI and STT are inventors of the PCT patents Cancer Diagnosis and Therapy (PCT/NZ2015/050108) and Cancer Therapeutic (PCT/NZ2018/050006), and provisional patent application Novel Pharmaceutical Compositions for Cancer Therapy (US/62/711709).

Funding

This research did not receive any grant from funding agencies in the public, commercial, or not-for-profit sectors.

Ethics approval

This study was approved by the Central Health and Disabilities Ethics Committee (Ref. no. 12/CEN/74).

Supplementary materials

Supplementary material associated with this article can be found, in the online version, at doi:10.1016/j.bjps.2018.11.013.

References

1. Brougham ND, Dennett ER, Cameron R, Tan ST. The incidence of metastasis from cutaneous squamous cell carcinoma and the impact of its risk factors. *J Surg Oncol* 2012;**106**:811–15.
2. Rudolph R, Zelac DE. Squamous cell carcinoma of the skin. *Plas Reconstr Surg* 2004;**114** 82e–94e.
3. Skulsky SL, O'sullivan B, McArdle O, et al. Review of high--risk features of cutaneous squamous cell carcinoma and discrepancies between the American joint committee on cancer and NCCN clinical practice guidelines in oncology. *Head Neck* 2017;**39**:578–94.
4. Nuño-González A, Vicente-Martín F, Pinedo-Moraleda F, López-Estebaranz J. High-risk cutaneous squamous cell carcinoma. *Actas Dermo-Sifiliográficas (English Edition)* 2012;**103**:567–78.
5. Baccelli I, Trumpp A. The evolving concept of cancer and metastasis stem cells. *J Cell Biol* 2012;**198**:281–93.
6. Bradshaw A, Wickremsekera A, Tan ST, et al. Cancer stem cell hierarchy in glioblastoma multiforme. *Front Surg* 2016;**3**:21.
7. Clevers H. What is an adult stem cell? *Science* 2015;**350**:1319–20.
8. Jordan CT, Guzman ML, Noble M. Cancer stem cells. *New Engl J Med* 2006;**355**:1253–61.
9. Yamanaka S. Induction of pluripotent stem cells from mouse fibroblasts by four transcription factors. *Cell Prolif* 2008;**41**: 51–56.
10. Schmidt C, Martin JM, Khoo E, Plank A, Grigg R. Outcomes of nodal metastatic cutaneous squamous cell carcinoma of the head and neck treated in a regional center. *Head Neck* 2015;**37**:1808–15.
11. Koh SP, Brasch HD, de Jongh J, et al. Cancer stem cells in moderately differentiated head and neck cutaneous squamous cell carcinoma. *Heliyon* 2019 (Accepted for publication).
12. Peach MJ. Renin-angiotensin system: Biochemistry and mechanisms of action. *Physiol Rev* 1977;**57**:313–70.
13. Atlas SA. The renin-angiotensin aldosterone system: Pathophysiological role and pharmacologic inhibition. *J Manag Care Pharm* 2007;**13**:9–20.
14. Ram RS, Brasch HD, Dunne JC, et al. Cancer stem cells in moderately differentiated lip squamous cell carcinoma express components of the renin-angiotensin system. *Front Surg* 2017;**4**:30.
15. Balyasnikova IV, Danilov SM, Muzykantov VR, Fisher AB. Modulation of angiotensin-converting enzyme in cultured human vascular endothelial cells. *In Vitro Cell Dev Biol Animal* 1998;**34**:545–54.
16. Ager EI, Neo J, Christophi C. The renin–angiotensin system and malignancy. *Carcinogenesis* 2008;**29**:1675–84.
17. Pinter M, Jain RK. Targeting the renin-angiotensin system to improve cancer treatment: Implications for immunotherapy. *Sci Trans Med* 2017;**9**:eaan5616.
18. Tan S, Itinteang T, Day D, et al. Treatment of infantile haemangioma with captopril. *Br J Dermatol* 2012;**167**:619–24.
19. Tan K, Brasch HD, van Schaijik B, et al. Expression and localization of Cathepsins B, D, and G in Dupuytren's disease. *Plast Reconstruc Surg Global Open* 2018;**6**:1668e.
20. Munro MJ, Wickremesekera AC, Davis PF, et al. Renin-angiotensin system and cancer: A review. *Integr Cancer Sci Ther* 2017;**4**:1–6.
21. Nguyen G, Delarue F, Burcklé C, et al. Pivotal role of the renin/prorenin receptor in angiotensin II production and cellular responses to renin. *J Clin Invest* 2002;**109**:1417.
22. George AJ, Thomas WG, Hannan RD. The renin–angiotensin system and cancer: Old dog, new tricks. *Nat Rev Cancer* 2010;**10**:745.
23. Hanahan D, Weinberg RA. The hallmarks of cancer. *Cell* 2000;**100**:57–70.
24. Nguyen L, Ager EI, Neo J, Christophi C. Regulation of colorectal cancer cell epithelial to mesenchymal transition by the renin angiotensin system. *J Gastroenterol Hepatol* 2016;**31**:1773–82.
25. Fan YL, Zheng M, Tang YL, Liang XH. A new perspective of vasculogenic mimicry: EMT and cancer stem cells. *Oncol Lett* 2013;**6**:1174–80.
26. Cima I, Kong SL, Sengupta D, et al. Tumor-derived circulating endothelial cell clusters in colorectal cancer. *Sci Trans Med* 2016;**8** 345ra89–345ra89.
27. Vinson GP, Barker S, Puddefoot JR. The renin–angiotensin system in the breast and breast cancer. *Endocr Relat Cancer* 2012;**19**:R1–R19.
28. Deshayes F, Nahmias C. Angiotensin receptors: A new role in cancer? *Trend Endocrinol Metab* 2005;**16**:293–9.
29. Takeda H, Kondo S. Differences between squamous cell carcinoma and keratoacanthoma in angiotensin type-1 receptor expression. *Am J Pathol* 2001;**158**:1633–7.
30. Tawinwung S, Ninsontia C, Chanvorachote P. Angiotensin II increases cancer stem cell-like phenotype in lung cancer cells. *Anticancer Res* 2015;**35**:4789–97.
31. Li C, Siragy HM. High glucose induces podocyte injury via enhanced (pro) renin receptor-Wnt-β-catenin-snail signaling pathway. *PLoS One* 2014;**9**:e89233.
32. Featherston T, Yu HH, Dunne JC, et al. Cancer stem cells in moderately differentiated Buccal Mucosal squamous cell carcinoma express components of the renin–angiotensin system. *Front Surg* 2016;**3**:52.
33. Itinteang T, Dunne JC, Chibnall AM, et al. Cancer stem cells in moderately differentiated oral tongue squamous cell carcinoma express components of the renin–angiotensin system. *J Clin Pathol* 2016;**69**:942–5.
34. Bradshaw AR, Wickremesekera AC, Brasch HD, et al. Glioblastoma multiforme cancer stem cells express components of the renin–angiotensin system. *Fron Surg* 2016;**3**:51.
35. Oh B-H, Mitchell J, Herron JR, et al. Aliskiren, an oral renin inhibitor, provides dose-dependent efficacy and sustained 24-hour blood pressure control in patients with hypertension. *J Am Coll Cardiol* 2007;**49**:1157–63.
36. Raskin P. Treatment of hypertension in adults with diabetes. *Clin Diabet* 2003;**21**:120–1.
37. Burnier M, Brunner H. Angiotensin II receptor antagonists. *Lancet* 2000;**355**:637–45.
38. Christian JB, Lapane KL, Hume AL, Eaton CB, Weinstock MA. Association of ACE inhibitors and angiotensin receptor blockers with keratinocyte cancer prevention in the randomized VATTC trial. *J Natl Cancer Inst* 2008;**100**:1223–32.